Journal of Power Sources 196 (2011) 5394–5401

Contents lists available at ScienceDirect

Journal of Power Sources

journal homepage: www.elsevier.com/locate/jpowsour

Composite membranes based on micro and mesostructured silica: A comparison of physicochemical and transport properties

A. Alvarez[a], C. Guzmán[a], A. Carbone[b,*], A. Saccà[b], I. Gatto[b], R. Pedicini[b], E. Passalacqua[b], R. Nava[c], R. Ornelas[d], J. Ledesma-García[c,**], L.G. Arriaga[a]

[a] Centro de Investigación y Desarrollo Tecnológico en Electroquímica, 76703 Querétaro, Mexico
[b] CNR-Istituto di Tecnologie Avanzate per l'Energia, Via S. Lucia sopra Contesse-5, 98126 Messina, Italy
[c] División de Investigación y Posgrado, Facultad de Ingeniería, Universidad Autónoma de Querétaro, 76010 Querétaro, Mexico
[d] TRE SpA – Tozzi Renewable Energy, Via Zuccherificio, 10-48010 Mezzano (RA), Italy

ARTICLE INFO

Article history:
Received 11 January 2011
Received in revised form 18 February 2011
Accepted 21 February 2011
Available online 26 February 2011

Keywords:
H_2/air PEFC
Composite Nafion® membranes
Micro-mesoporous silica
Proton conductivity measurements

ABSTRACT

The aim of this work is to incorporate inorganic compounds into the Nafion matrix (composite membranes) for high temperature of a polymer electrolyte fuel cell (T_{cell} > 100 °C). Three silicon oxides having a different morphology were synthesized starting with a tetraethyl orthosilicate as a precursor via sol–gel method: SBA15, SBA15-SH and SiO_2. Successively, composite Nafion membranes were prepared using a 3% (w/w) of each powder through a standardized casting method. The influence of SiO_2 morphology on chemical–physical properties of the membranes was highlighted resulting in a reduction of the swelling parameters of the composite membranes if compared at $T \geq 80$ °C to a recast bare Nafion membrane, used as a reference. Good proton conductivity was also observed for all composite membranes with values of 0.144 S cm^{-1}, 0.136 S cm^{-1}, 0.090 S cm^{-1} and 0.078 S cm^{-1} recorded at 80 °C (100% RH) for Nrecast, NSBA15, NSBA15-SH and $NSiO_2$, respectively. The polarisation curves carried out at 120 °C (75% RH, 1.5 abs. bar) have revealed a higher stability for NSBA15 membrane after a short time-test, probably because the silica morphology is able to retain water within the polymer matrix and, in accordance to the swelling data.

1. Introduction

Polymer electrolyte fuel cells (PEFCs) are a highly efficient technology and an environmentally attractive source for power generation in various applications such as stationary, military or portable devices and for this reason, in the last few years, they have received a special attention due to their high efficiency and low environment impact. In particular, the main attempts consist in the increase of the working temperature than a conventional one (T = 80 °C) because, operating at higher temperatures, it is possible to have a faster heat rejection rate, an easier and more efficient water management, a higher reaction rate and improved CO tolerance by the anode electrocatalysts.

Actually, Nafion® (perfluorosulphonic acid – PFSA) is the most widespread polymer used as an electrolyte for PEFC due to its properties such as high proton conductivity, good chemical resistance and mechanical properties. The ideal working temperature of a PEFC that uses a PFSA as an electrolyte is fixed at about 80 °C because, at this temperature and at atmospheric pressure, the proton conduction mechanism of Nafion® is water assisted. In fact, the water contained in the sulphonic clusters changes its state in a vapor phase producing a lack in the proton conductivity and, consequently, the electrochemical performance drastically falls [1–7].

In the last few years, the Nafion® structure has been modified through different methods, for example, including inorganic oxides and/or proton conductors within the polymer matrix [8] to maintain good proton conductivity at higher temperatures overcoming the operating temperature limitation of the fuel cell, to improve water retention at T > 100 °C, to maintain the mechanical properties of the polymer chain, in order to be prevent its degradation. Inorganic oxides are widely used due to their hygroscopic properties and their capability to retain water molecules in their environment through ionic dipoles. On the other hand, inorganic oxides supply a major mechanical stiffness to the membrane structure and reduce the permeation of fuel since they induce a certain tortuosity in the pathway within the polymeric matrix. Several previous studies on composite membrane development have shown that water retention capability is greater at higher temperatures and the filler presence improves the thermal properties and mechanical stabil-

* Corresponding author.
** Corresponding author. Tel.: +52 442 1921200x65411; fax: +52 442 1921200x65411.
E-mail addresses: carbone@itae.cnr.it (A. Carbone), janet.ledesma@uaq.mx (J. Ledesma-García).

0378-7753/$ – see front matter © 2011 Elsevier B.V. All rights reserved.
doi:10.1016/j.jpowsour.2011.02.072

ity, extending the operating range of both the membrane and the fuel cell [9–14].

In recent years, mesoporous silica materials have attracted considerable attention because they possess a high surface area and a hexagonal arrangement of uniform pores. Recently, several papers have been devoted to the modification of mesoporous silica with functional groups and the characterization of its spectroscopic and structural properties, identifying this material as a template to produce other helpful materials [2,9]. In such a context, the present paper describes the Nafion® polymer modification using three different silicon oxides: a microporous SiO_2 (named SiO_2), a mesoporous SBA-15 silica (named SBA15), and a SBA15 silica functionalized with –SH groups (named SBA15-SH) in order to strengthen the membrane and to increase proton conductivity at higher temperatures. A series of composite membranes containing the microporous SiO_2 and two different mesoporous SiO_2 (SBA15 and SBA15-SH) were prepared and characterised in terms of water uptake (Wup, %), ion exchange capacity (IEC, mequiv. g^{-1} SO_3H), dimensional analysis to define the swelling parameters, X-ray diffraction analysis, Fourier transform infrared (FT-IR) spectroscopy, micro Raman spectroscopy. The electrochemical characterization was carried out both in terms of proton conductivity (30–120 °C, 100% RH) and *I–V* curves in a commercial single cell feeding by H_2/air in the temperature range between 80 and 120 °C at different humidification values (100 and 75% RH). The results in terms of polarisation curves have been evaluated and compared to a recast bare Nafion membrane of comparable thickness.

2. Experimental

2.1. Synthesis of inorganic fillers

Microporous silica (named SiO_2 in the text) was synthesized via a sol–gel method under acidic conditions. A tetraethyl orthosilicate (TEOS, 98%, Aldrich) as a precursor was employed using a HNO_3 solution with a molar ratio 1:1 as a catalyst. This colloidal solution was kept at room temperature until it reached a solid formation. The resulting solid was thermally treated using a tubular furnace (Barnstead Thermolyne) at 150 °C for 2 h in order to remove the residual alcohol and obtain the oxide of silicon [15–21].

For the synthesis of SBA-15 material, the Pluronic P123 triblock copolymer (BASF Corporation) was used as a surfactant structure directing agent. It was dissolved in a 4 M HCl solution under stirring. Then the required amount of TEOS was added to the solution and stirred at 35 °C for 24 h. The resulting slurry was transferred into polypropylene bottles and heated at 80 °C in an oven for 24 h. The solid products were filtered and washed with deionised water, air dried at room temperature for 24 h and at 110 °C for 18 h, then calcined at 500 °C for 6 h in order to remove the organic template [22–25].

The surface modification of SBA-15 with mercaptan groups was performed by a post-synthesis method (ex situ) starting with the previously synthesized SBA-15. The mesoporous silica (2.3 g) was dispersed in a solution of 3-mercaptopropil trimethoxysilane (2.2 ml) and 2-propanol under stirring for 45 min in an inert atmosphere at room temperature. The solid products were filtered and washed with deionised water, air dried at room temperature for 24 h and, finally, dried at 110 °C for 24 h [26,27].

2.2. Preparation of composite membranes

A 5% (w/w) Ion Power Nafion® alcoholic solution (LQ1105) was selected to manufacture the film. The original solution was desiccated at T = 40 °C under vacuum using a rotating evaporator until obtaining a dry residue, successively solubilised in dimethylacetamide (DMAc) as a solvent in order to obtain a 20% (w/w) solution. Such a solution was used to prepare a recast bare membrane (Nrecast), used as a reference, and three different composite membranes ($NSiO_2$, NSBA15 and NSBA15-SH) using the corresponding silica powders. All the membranes were prepared using the Doctor blade technique. For each composite membrane, an amount of 3% (w/w) of oxide powder compared to the dry Nafion resin was added to 20% (w/w) polymeric solution and dispersed in an ultrasonic bath for 30 min before the re-concentration phase necessary for the casting procedure. Through a slow re-concentration at 80 °C under a magnetic stirring, suitable viscosity solutions were obtained and stratified on a glass sheet. The obtained membranes were dried on the hot plate at T = 80 °C for 3 h to evaporate the solvent and, then, detached from the glass with distilled water. Successively, they underwent a thermal treatment until T = 155 °C (30 min) to enhance the crystalline phase of the polymer and, consequently, to improve the mechanical properties [28,29]. A chemical treatment in HNO_3/H_2O (1:1, vol.) at 80 °C for 30 min was carried out for all membranes, except for the NSBA15-SH membrane which was treated in H_2O_2 (30 wt%) at 80 °C for 30 min, instead of nitric solution, with the aim of oxidizing the SH groups to SO_3H groups. An intermediate boiling step in distilled water was used (15 min) and a treatment in a 1 M H_2SO_4 solution at 80 °C for 30 min was employed for all the membranes with final washing steps in boiling distilled water (3 times – 15 min each). This chemical treatment permits the films to be purified from eventual impurities and obtain a high wettability of the developed membranes. Membranes having a comparable thickness (110–120 μm) were prepared and used both for the chemical–physical and electrochemical characterization.

2.3. Characterization of fillers and membranes

2.3.1. Physicochemical characterization of inorganic fillers

The textural properties of the inorganic fillers were determined through the adsorption–desorption isotherms of N_2 at 77 K on a Micromeritics TriStar 3000. The surface area of the samples was calculated according to the BET (Brunauer–Emmett–Teller) equation. The prepared oxides were characterized by X-ray powder diffraction (XRD) analysis performed using a Philips X-ray automated diffractometer (model PW3710) with the Cu Kα radiation in the range $5° < 2\theta < 100°$. Fourier transform infrared (FT-IR) spectra were collected using a Bruker (Vector 33), in the spectral range of 400–4000 cm^{-1} for the transmission mode, while 4000–400 cm^{-1} for the ATR. The morphology of the powder was observed using a Hitachi S-4800 FE-SEM (field emission scanning electron microscopy) and a high-resolution transmission electron microscope (HRTEM) JEOL JEM-2000FX FASTEM operating at 200 kV with a very low light to avoid the damage of the material under the electron beam. The thermo-gravimetric analysis (TGA) was carried out with a 2950 TGA HR V5.4TA in air following the variation of the percentage weight loss, in the range between room temperature and 600 °C with a temperature rate of 5 °C min^{-1}.

2.3.2. Composite membrane characterization

2.3.2.1. Physicochemical methods. Micro-Raman spectra were recorded using a commercial micro-Raman system Bruker (Senterra). All Raman spectra were recorded at room temperature. The morphology of the composite membranes was observed by scanning electron microscopy (SEM) in a JEOL JSM-6060 LV microscope and the surface mapping by energy dispersive X-ray spectroscopy (EDXS). The XRD, FT-IR analyses were performed similarly to the analyses employed on the inorganic fillers as mentioned in Section 2.3.1.

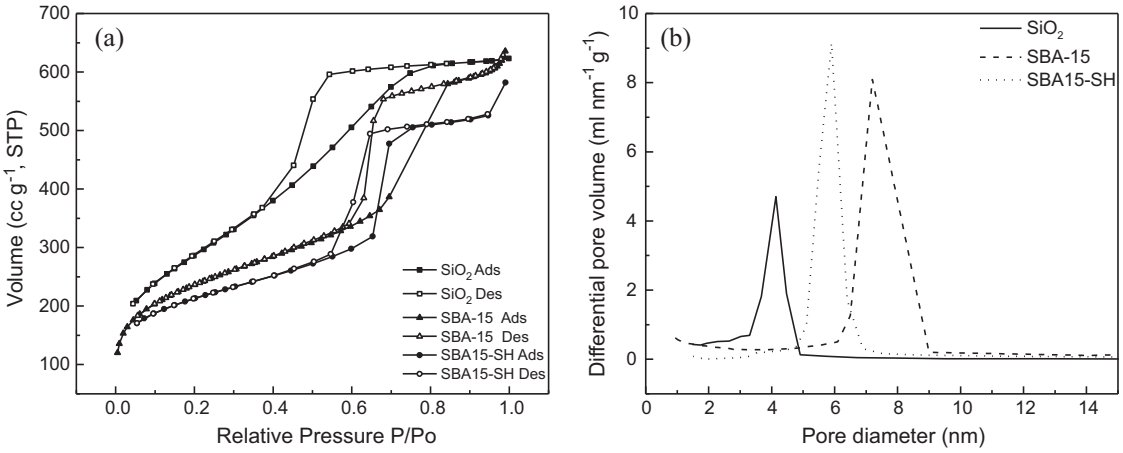

Fig. 1. (a) Nitrogen adsorption–desorption isotherms at 77 K of inorganic fillers. (b) The corresponding pore size distribution of fillers determined from adsorption of the N_2 isotherms.

2.3.2.2. Ionic exchange capacity (IEC) and water uptake measurements. The IEC of the membranes was determined through an acid–base titration with an automatic titrator (Metrohm, mod. 751 GPD Titrino). At first, the membranes were desiccated at 80 °C for 2 h in oven under vacuum to determine the dried weight. Successively, they were immersed in a 1 M NaCl solution to exchange the H^+ of the SO_3H group with Na^+ and the solution was titred through a 0.01 M NaOH solution to neutralize the exchanged H^+. Taking into account the dry weight of each sample and plotting the pH variation with the added titrant volume, the latter at the equivalent point was determined. The IEC of the membrane (IEC_m) is calculated using the following formula:

$$IEC_m = \frac{V \times M}{m_{dry}} \quad (1)$$

where IEC is the ionic exchange capacity expressed in SO_3H mequiv. g^{-1}; V, the added titrant volume at the equivalent point expressed in ml; M, the molar concentration of the titrant; m_{dry} is the dry mass of the sample expressed in g. In order to evaluate the contribution of the inorganic filler onto the ionic exchange capacity, the IEC of the polymer (IEC_p) for the composite membrane was calculated following the equation [30]:

$$IEC_p = \frac{IEC_m}{PF} \quad (2)$$

where IEC_m is expressed from Eq. (1) and PF represents fraction of polymer in the membrane.

The water uptake (Wup, %) was determined by the difference between the wet and the dry mass of the membrane. The dry mass was calculated maintaining the samples in an oven under vacuum at 80 °C for 2 h, while the wet mass was determined swelling the samples in distilled H_2O at room temperature for 24 h. To obtain the Wup at 80 °C and 95 °C the sample was maintained in distilled water for 2 h, respectively to have the swelling behaviour at the corresponding temperatures, always through the weight difference between dry/wet samples [14,28,29]. The formula used is:

$$Wup\ (\%) = \frac{M_{wet} - M_{dry}}{M_{dry}} \times 100 \quad (3)$$

where M_{wet} and M_{dry} are the wet and dry weights at the corresponding temperatures.

2.3.2.3. Proton conductivity measurements. The proton conductivity measurements of the membranes were carried out in a hydrogen atmosphere with a four-electrode method and in a DC current by using a commercial conductivity cell (Bekktech) and a potentiostat–galvanostat (AMEL mod 2049). The membrane proton conductivity was determined as a function of the temperature (from 30 to 120 °C) at a relative humidity of 100% [29].

2.4. Electrochemical characterization of the composite membranes

2.4.1. Electrodes and MEA preparation

The electrodes were prepared by spray technique as described elsewhere [31]. The catalytic layer was obtained by mixing a 50% (w/w) Pt/C (Johnson Mattey) as an electro-catalyst with a 33% (w/w) Nafion alcoholic solution (Aldrich, 5%, w/w), 20% (w/w) of ammonium carbonate (Carlo Erba) as a pore-former. A Pt loading of 0.1 and 0.4 mg cm^{-2} at the anode and the cathode sides, respectively was used. The catalytic ink was sprayed on a PTFE support and dried up at 125 °C in order to obtain the catalytic layer. The developed catalytic layer was applied, through a decal technique, onto the membrane to obtain the Catalyst Coated Membrane (CCM). The MEAs were obtained by hot-pressing the Gas Diffusion Layers (GDLs) by a standardized procedure described elsewhere [31] onto the CCM. A 42 μm adhesive polyester sheet was used as a pre-gasket.

2.4.2. Electrochemical characterization in single cell

Electrochemical tests were carried out in a 25 cm^2 commercial single cell connected to a commercial work station. MEAs fabricated with the different developed membranes were tested in a range of 80 °C < T < 120 °C in humidified H_2/air gases at 1.5 abs. bar varying the relative humidity between a 100% RH value (80–100 °C) and 75% RH (110–120 °C). The gas fluxes were fixed at 1.5 times the stoichiometric value for the fuel and 2 times the stoichiometric value for the oxidant at a current density value of 1 A cm^{-2}. The polarisation curves were recorded by means of a test station equipped with software for the automatic data acquisition and the cell resistance was measured with an Agilent milliohmmeter by a static method at a frequency of 1 kHz.

3. Results and discussion

3.1. Characterization of inorganic fillers

Fig. 1a shows the nitrogen sorption isotherms of the mesoporous silica samples and the pore size distribution derived from adsorption and desorption branches of nitrogen isotherms (Fig. 1b). It can be seen that BET specific surface area of the inorganic fillers is slightly different with a value of 1039 m^2 g^{-1} for SiO_2 and a pore

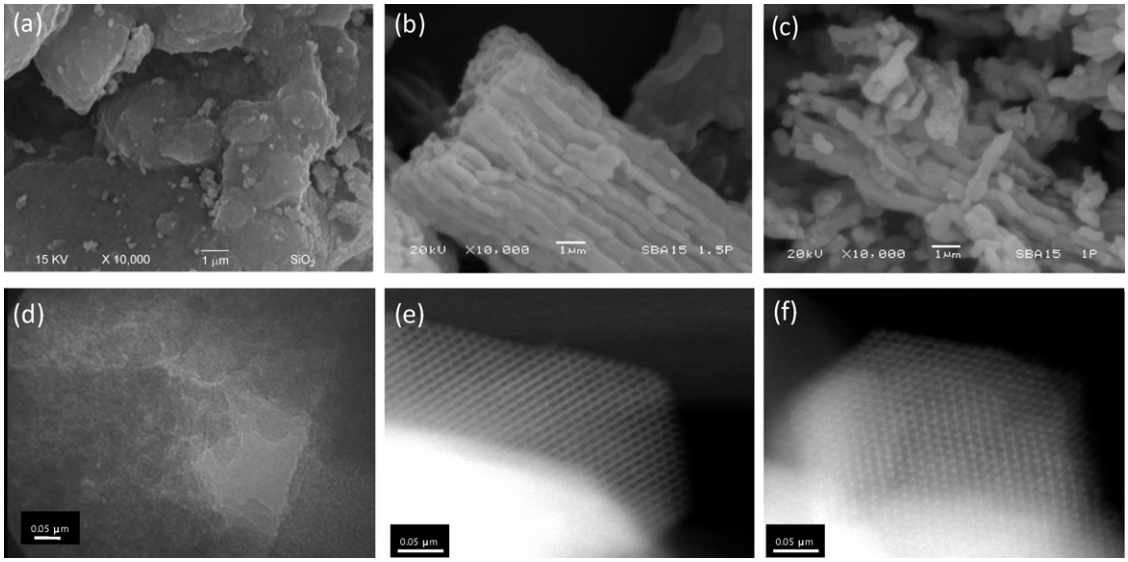

Fig. 2. SEM images of inorganic fillers: (a) SiO_2; (b) SBA-15; (c) SBA15-HS. TEM images of inorganic fillers: (d) SiO_2; (e) SBA-15; (f) SBA15-HS.

diameter that is only a little smaller (4 nm) indicating a significant formation of agglomerates and a non homogeneous morphology (Fig. 2a); the SBA-15 and SBA15-HS have an area of 932 $m^2\,g^{-1}$ and 737 $m^2\,g^{-1}$ with a pore diameter of 7 and 6 nm, respectively and a cylinder form with a highly uniform size of approximately 400–500 nm in diameter and of about 1–1.2 μm long (Fig. 2b and c) [32]. These results confirm that the pore diameter and BET surface area for the inorganic fillers are not dependant on the silica source, but they are dependant on the nature of the directing agent (Pluronic P123) and its associated cosolvent that induce the mesostructure formation, which produces an hexagonal arrangement with a pore diameter between 7 and 6 nm (SBA-15 and SBA15-HS) [33].

From the TEM images also presented in Fig. 2, it is clear that SiO_2 powder has got a non-homogeneous morphology with a particle size distribution of approximately 4 nm (Fig. 2d). For SBA-15 and SBA15-HS modified through thiol groups, a hexagonal arrangement of uniform pores (Fig. 2e) was found, indicating that the mesopores of the SBA-15 were not destroyed after the modification occurred through the mercaptan groups (Fig. 2f) [32,34,35].

Fig. 3 reports the X-ray diffraction patterns of SiO_2, SBA-15 and SBA15-HS materials. It can be observed a broad reflection peak centered at about $2\theta = 24^\circ$, characteristic of amorphous silica (SiO_2) [36].

Fig. 4 shows the FT-IR spectrum of mesoporous silica SBA-15 and SBA15-SH modified with mercaptan groups, which has got a typical spectrum of silica. The bands at 811 and 1087 cm^{-1} belong to the symmetrical and asymmetrical vibrations of the bond Si–O–Si. The band at 463 cm^{-1} has been assigned to the torsion vibration of the bond Si–O–Si. The band at 967 cm^{-1} belongs to the vibration of silanol group (Si–OH). The band at 1635 cm^{-1} corresponds to free H_2O. Finally, the intensive and broad band centered at 3442 cm^{-1} is assigned to the superposition of vibrations related both to the physically adsorbed H_2O and the silanol groups. The IR spectrum of SBA-15 surface modified with mercaptan groups shows the characteristic bands corresponding to the vibration of SH bonds (2574 cm^{-1}). The previous assignments were made based on those reported in the literature [36,37]. The bands characteristic of the SH group cannot be observed in Fig. 4, because they have a low vibrational energy and concentration, so a trial was conducted on the SBA15-SH functionalized in the presence of hydrogen per-

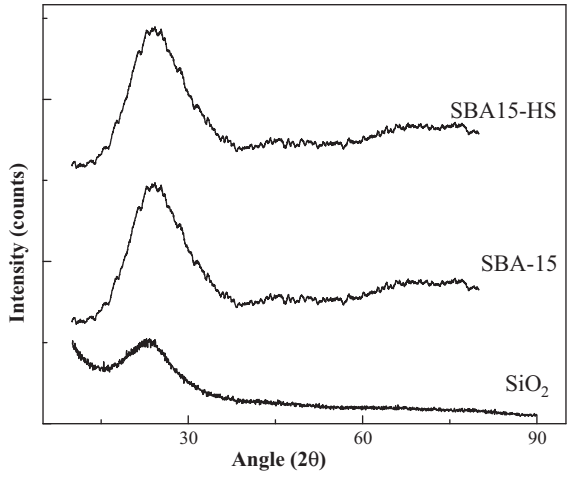

Fig. 3. X-ray diffraction patterns of inorganic fillers.

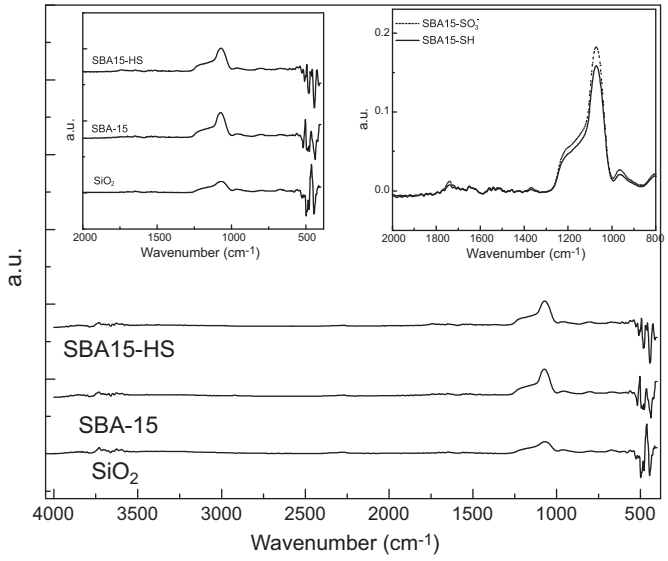

Fig. 4. Representative FT-IR spectroscopy of the inorganic fillers.

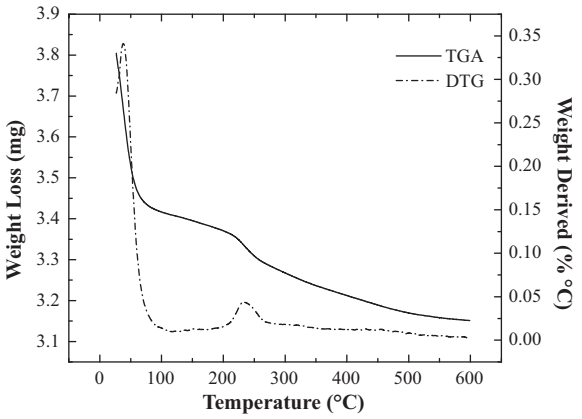

Fig. 5. Thermo-gravimetric analyses of SBA15-SH.

oxide in order to oxidize SH to SO_3^- groups. In the inset of Fig. 4, the increase in the band 1055 cm^{-1}, assigned to the presence of Si–O–Si and SO_3^-, is visible. These two bands are overlapped, so only the rise of this band is noticeable when it is functionalized.

The thermal stability of SBA15-SH was analyzed by TGA as shown in Fig. 5. The weight loss from 100 °C to 300 °C corresponds to the evaporation of the water absorbed by silica [2]. The DTG of SBA15-SH only exhibits one distinct decomposition region at about 235 °C, mainly attributable to the thermal decomposition of mercaptan and metilen groups.

3.2. Physicochemical properties of composite membranes

Fig. 6 shows the SEM images of the composite membranes. The backscattered electron images and EDXS mapping images of (a) $NSiO_2$, (b) NSBA-15 and (c) NSBA15-SH surfaces also are presented in Fig. 6. The EDX spectra allowed the elements present in the membranes to be determined. EDXS mapping illustrates the distribution of a chosen element across the image. EDXS dot mapping was performed on each membrane for fluorine (Fig. 6a-II, b-II and c-II) and silicon atoms (Fig. 6a-III, b-III and c-III). As expected, fluorine is observed in all the membranes. The dispersion of the inorganic filler is homogeneous, with the formation of a minimal agglomeration of the material on the membrane.

With the aim of determining if the formed nanoparticles are in a crystalline state in the composite membranes, X-ray diffraction (XRD) measurements on recast Nafion® membrane and composite membranes were performed and the corresponding diffraction patterns are shown in Fig. 7. The composite membranes have a XRD pattern similar to the recast Nafion®, indicating no crystalline silica particle formation [38]. It is clear that recast Nafion® as well as composite membranes show peaks at 18° and 39.3° 2θ which

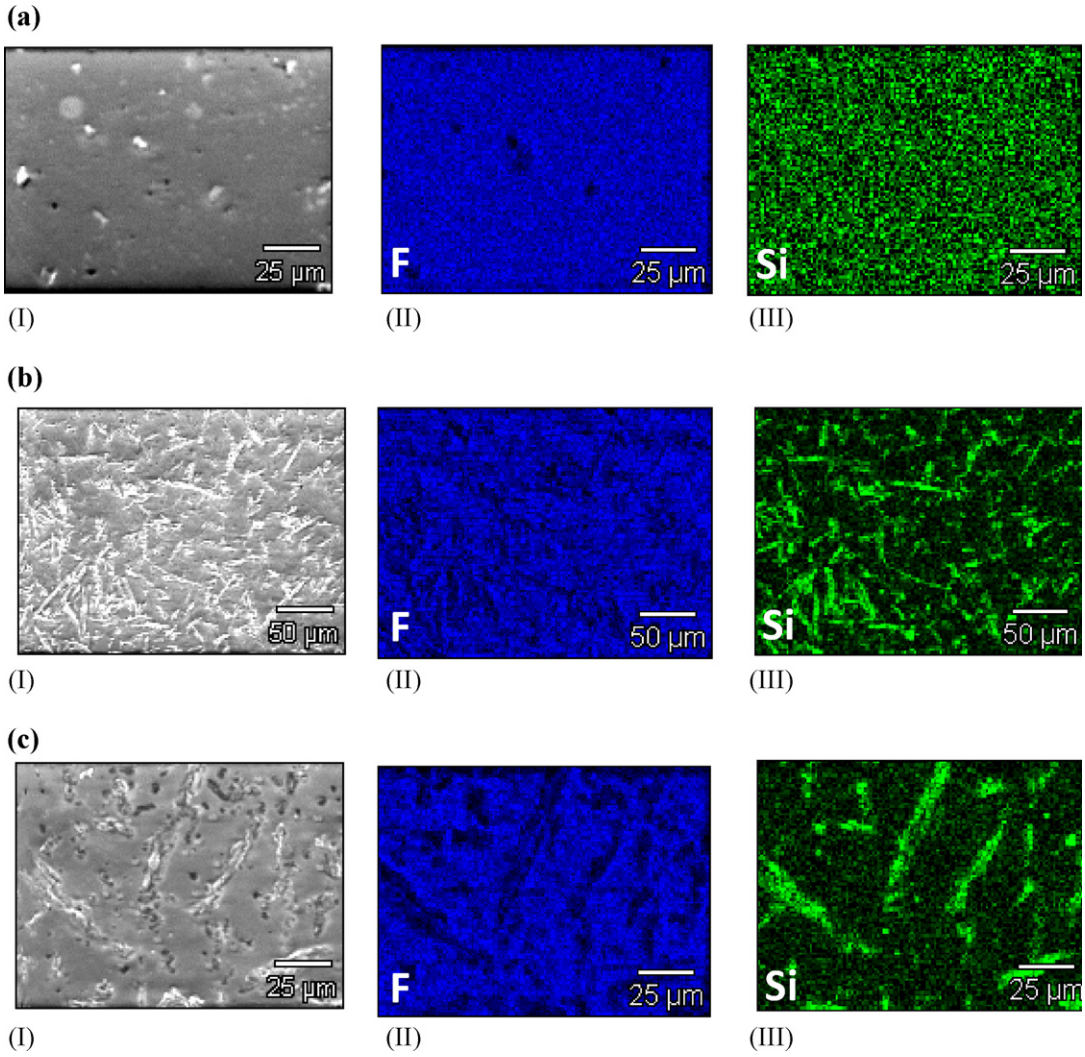

Fig. 6. (I) SEM images, (II) EDXS mapping of fluorine and (III) EDXS mapping image of Si, for (a) $NSiO_2$, (b) NSBA-15, and (c) NSBA15-SH membranes.

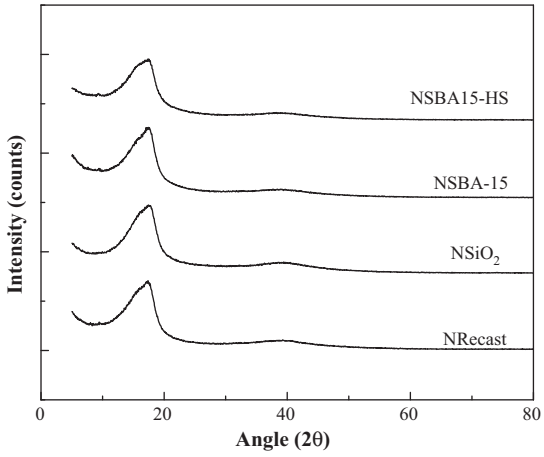

Fig. 7. X-ray diffraction results of the membrane surface of recast Nafion® and composite membrane.

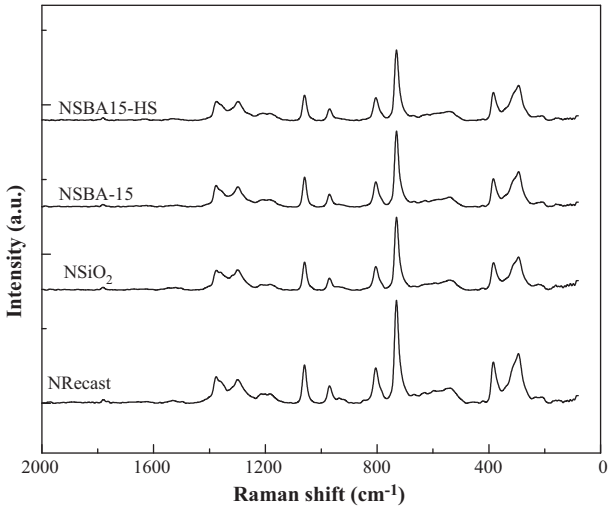

Fig. 9. Micro-Raman spectra of composite membranes.

can be attributed to the semi crystalline polyfluorocarbon chain of Nafion® [7,39–41].

Fourier transform infrared spectra at wave numbers 4000–600 cm^{-1} for the composite membranes have been recorded, analyzed and compared to the Nrecast membrane. IR spectra for all the composite membranes are presented in Fig. 8. The spectra have indicated a peak shift for the composite membranes due to the change in the inorganic fillers content. In the recast Nafion® membrane, the two major vibrational structures at 1199 cm^{-1} and 1146 cm^{-1} for CF_2 stretching vibration of the PTFE backbone can be observed. The peaks observed at 1055 and 967 cm^{-1} are attributed to the stretching vibration moieties of $SO3^-$ and C–O–C, respectively [42]. The peak of Si–O–Si is revealed at a wave number of 1063 cm^{-1}, while the Si–OH stretching vibrations in the composite membrane are observed at a wave number of 961 cm^{-1}. The used silica particles possess abundant hydroxyl groups as shown by the absorption peak at 3440 cm^{-1} [42,43].

In the micro-Raman spectrum, reported in Fig. 9, the band 968 cm^{-1} is attributed to the symmetric C–O–C. The bands peaking at 500–1220 cm^{-1} presents the bending vibrations typical of CF_2; the band at 1060 cm^{-1} corresponds to the vibration of the acid groups SO^{3-}, while the vibration at 535 cm^{-1} was assigned to the Si–O–Si symmetric bending; at the end, the intensity of peaking at 1060 cm^{-1} is associated to the Si–O–Si and SO^{3-} vibrations, strongly overlapped [42,43].

The water uptake values of composite membranes and recast Nafion® at 95 °C are gathered in Fig. 10. Recast Nafion® membrane has a higher water uptake if compared to the composite membranes. The membrane properties (structural properties, ionic-domain organization, etc.) may be modified by the casting procedure and incorporation of the inorganic fillers. The swelling parameters of composite membranes are lower than those of Nrecast at 95 °C. In particular, the water uptake for NSBA-15 is lower than $NSiO_2$ and this value is increased when the functional groups are introduced (NSBA15-SH). The most interesting characteristic consists of the water distribution inside the membrane which is influenced by the silica morphology. In fact, the volume variation is predominant compared to the area variation for NSBA15 and NSBA15-SH and vice versa for $NSiO_2$. It seems that when tubular silica is used, the swelling occurs along the thickness, while using spherical silica, it happens along the surface.

Ion exchange capacities of recast Nafion® and composite membranes, as measured by titration, are shown in Table 1. In general, the IEC of composite membranes is lowered by the presence of an inert inorganic material not participating in the ionic exchange, but in the case of functionalized silica (NSBA15-SH) the IEC further decreases, meaning that no additive SO_3H group was created

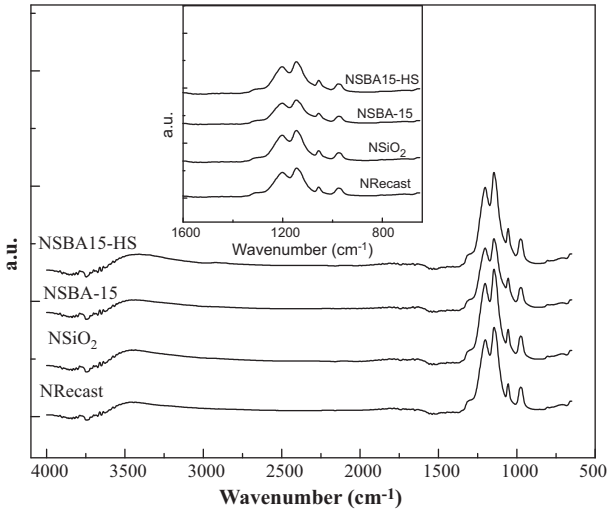

Fig. 8. Fourier transforms infrared (FT-IR) spectra of recast Nafion® and composite membrane.

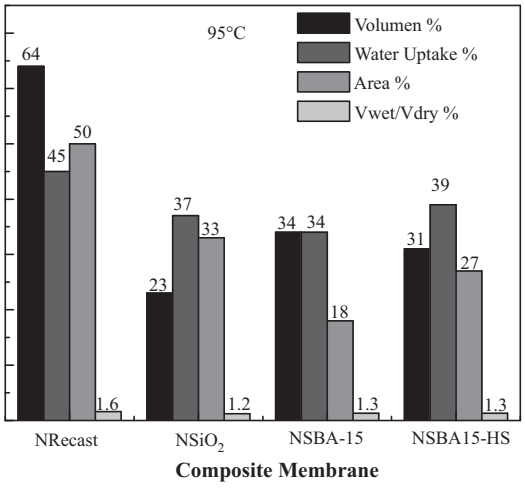

Fig. 10. Swelling behaviour at $T = 95$ °C.

Table 1
IEC of composite membranes.

Membrane	IEC_m (mequiv. g^{-1})	IEC_p (mequiv. g^{-1})
Nrecast	1.01	1.01
$NSiO_2$	0.96	0.99
NSBA15	0.97	1.0
NSBA15-HS	0.94	0.97

Table 2
Proton conductivity values at 30 °C and 100% RH.

Membrane	σ (S cm^{-1})
Nrecast	0.093
$NSiO_2$	0.061
NSBA-15	0.100
NSBA15-HS	0.079

through the treatment in H_2O_2 30% (w/w) used for NSBA15-SH membrane, because the powder is encapsulated into the polymeric matrix.

Moreover, the SH groups of SBA15-HS probably interact with the SO_3H groups of Nafion rendering them inactive for the IEC [30].

3.3. Electrochemical behaviour of the composite membranes

The proton conductivity was measured at different temperatures. At 30 °C with a 100% RH, as reported in Table 2, the $NSiO_2$ membrane shows proton conductivity lower than the Nrecast membrane in accordance with the IEC results. Contrarily, the NSBA-15 membrane containing the cylindrical silica, presents proton conductivity comparable to Nrecast, despite the lower IEC. Since IEC_p of $NSiO_2$ and NSBA15 is the same as the Nrecast membrane meaning that all sulphonic groups of Nafion are disposable, such observable difference in the proton conductivity values is attributable to the different morphology of the filler in accordance to the swelling data. In particular, for the cylindrical silica of NSBA15, the conduction path is not hindered by a different disposal of the silica particles. Further functionalization through thiol groups (NSBA15-SH) reduces the proton conductivity due to the interaction of SH groups with the sulphonic groups.

The proton conductivity as a function of the temperature was measured at RH = 100% and is reported in Fig. 11. When the temperature is increased until 120 °C, the membrane behaviour is analogous to that at a low temperature with a slight increase in terms of proton conductivity over 80 °C. An interesting trend is supplied by the composite membrane NSBA15-SH containing the functionalized mesoporous silica with a noticeable increase in the proton conductivity at $T > 80$ °C until reaching the Nrecast and NSBA15 values at 110 and 120 °C. This could be attributable to a higher swelling of the membrane that provokes a possible re-activation of sulphonic groups of Nafion.

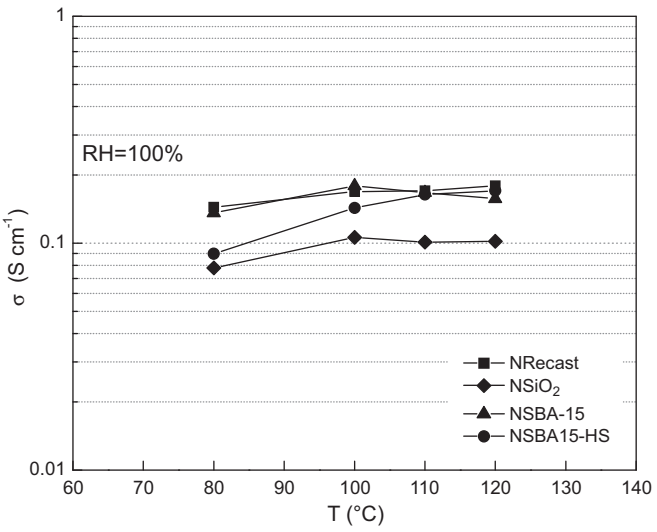

Fig. 11. Proton conductivity at RH = 100% as a function of temperature.

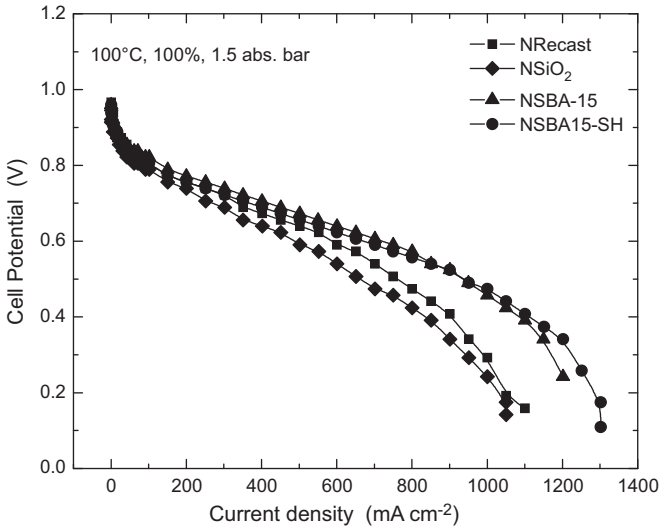

Fig. 12. Polarisation curves at 100 °C, 100% RH, 1.5 abs. bar.

Furthermore, the electrochemical characterization in terms of the *I–V* curve was carried out as described in Section 2.4.2. In general, extremely elevated OCV values (0.950–0.980 V) were recorded in the whole condition range for all membranes revealing a good stiffness of the manufactured films at elevated temperatures, too. Regarding the *I–V* curves, the trend observed in the proton conductivity measurements was confirmed by single cell tests in the whole investigated temperature range. In general, composite membranes having the highest proton conductivity show the highest electrochemical performance. In particular, for NSBA15-SH, this trend is in accordance with the chemical–physical and proton conductivity data at 100 °C, a temperature at which the swelling process is more pronounced and the interaction between SH and SO_3H groups falls. As a consequence, the fuel cell performance increases with the increase of the cell temperature reaching the performance of NSBA15. In Fig. 12, the polarisation curves at 100 °C with fully humidified gases and low pressure are shown. It is evident that the silica morphology affects the *I–V* curve behaviour. In fact, the membrane containing the spherical silica ($NSiO_2$) presents a similar performance to the recast membrane with a limiting current of 1050 mA cm^{-2} against an 1100 mA cm^{-2} value, respectively. On the contrary, the membranes having the tubular silica as a filler have shown the highest performance with a limiting current of 1200 mA cm^{-2} (NSBA-15) and 1300 mA cm^{-2} (NSBA15-SH).

Successively, with the aim of validating the effect of the filler introduction on the electrochemical membrane stability, polarisation curves at 120 °C and reduced humidity (75% RH) were recorded before and after a short time test of 2 h (Fig. 13). Before the time test, the membranes containing the tubular silica (NSBA15 and NSBA15-SH) and the recast membrane have a similar performance, while the $NSiO_2$ shows a more resistive curve. After the short time test, the trend is completely different; in fact, all membranes drastically reduce their performance, except the NSBA-15. This membrane has

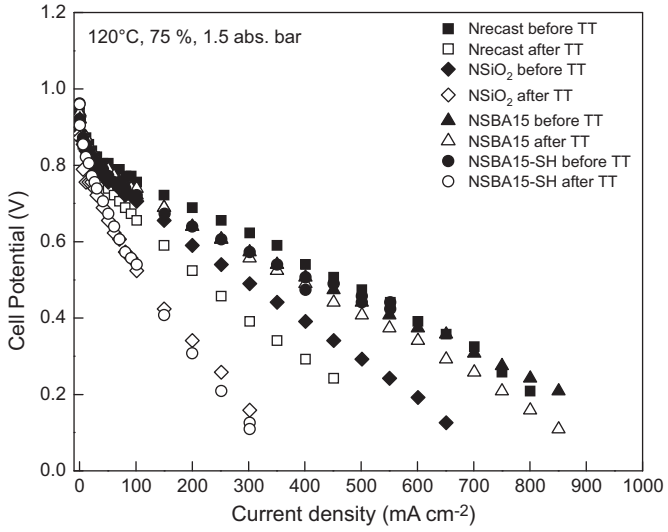

Fig. 13. Polarisation curves at 120 °C, 75% RH, 1.5 abs. bar.

shown the best stability in terms of performance drop, because the silica morphology is able to retain water within the polymer matrix, probably reducing the swelling phenomenon and stabilising the fuel cell performance as a function of the time. On the contrary, despite the SBA15-SH possessing a tubular morphology, the interaction SH–SO_3H is helpful at a temperature lower than 100 °C, but not at a temperature over 100 °C, whereas such interaction falls causing a further weakening of the membrane structure.

4. Conclusions

Composite membranes based on the use of silicon oxides with a different morphology were prepared and characterized in terms of the physicochemical and transport properties in a single cell. Under conditions of fully humidified gases, low pressure and 100 °C the composite membranes containing the tubular silica as a filler showed the highest performance with a limiting current of 1200 mA cm^{-2} (NSBA-15) and 1300 mA cm^{-2} (NSBA15-SH). However, at 120 °C and reduced humidity (75% RH) polarisation curves before and after a short time test of 2 h were recorded. After that time, the composite membrane NSBA-15 showed the best stability in terms of performance drop, due to the silica morphology which is able to retain water within the polymer matrix, probably reducing the swelling phenomenon and stabilising the fuel cell performance as a function of the time. Although, the SBA15-SH also possesses a tubular morphology, the interaction SH–SO_3H is helpful at a temperature up to 100 °C.

Acknowledgments

The authors thank the Mexican Council for Science and Technology CONACYT for financial support through Fomix-Zacatecas Grant 81728 and SEP-CONACYT 2009-133310. A. Alvarez also acknowledges CONACYT for a graduate scholarship.

References

[1] J. Yuan, G. Zhou, H. Pu, J. Membr. Sci. 325 (2008) 742–748.
[2] J. Wu, Z. Cui, C. Zhao, H. Li, Y. Zhang, T. Fu, H. Na, W. Xing, Int. J. Hydrogen Energy 34 (2009) 6740–6748.
[3] G. Gnana Kumar, A.R. Kim, K. Suk Nahm, R. Elizabeth, Int. J. Hydrogen Energy 34 (2009) 9788–9794.
[4] J. Sauk, J. Byun, H. Kim, J. Power Sources 143 (2005) 136–141.
[5] M.P. Rodgers, Z. Shi, S. Holdcroft, J. Membr. Sci. 325 (2008) 346–356.
[6] K. Wang, S. McDermid, J. Li, N. Kremliakova, P. Kozak, C. Song, Y. Tang, J. Zhang, J. Zhang, J. Power Sources 184 (2008) 99–103.
[7] K. Tae Park, U. Ho Jung, D. Woong Choi, K. Chun, H. Mee Lee, S. Hyun Kim, J. Power Sources 177 (2008) 247–253.
[8] J. Pan, H. Zhang, W. Chen, M. Pan, Int. J. Hydrogen Energy 35 (2010) 2796–2801.
[9] Y.F. Lin, C.Y. Yen, C.C.M. Ma, S.H. Liao, C.H. Lee, Y.H. Hsiao, H.P. Lin, J. Power Sources 171 (2007) 388–395.
[10] M. Helen, B. Viswanathan, S. Srinivasa Murthy, J. Membr. Sci. 292 (2007) 98–105.
[11] V. Antonucci, A. Di Blasi, V. Baglio, R. Ornelas, F. Matteucci, J. Ledesma-Garcia, L.G. Arriaga, A.S. Aricò, Electrochim. Acta 53 (2008) 7350–7356.
[12] A.S. Aricò, V. Baglio, A. Di Blasi, P. Creti, P.L. Antonucci, V. Antonucci, Solid State Ionics 161 (2003) 251–265.
[13] V. Baglio, A.S. Aricò, A. Di Blasi, V. Antonucci, P.L. Antonucci, S. Licoccia, E. Traversa, F. Serraino Fiory, Electrochim. Acta 50 (2005) 1241–1246.
[14] A. Sacca, I. Gatto, A. Carbone, R. Pedicini, E. Passalacqua, J. Power Sources 163 (2006) 47–51.
[15] J. González-Hernández, J.F. Pérez Robles, F. Ruiz, J.R. Martínez, Superficies y Vacío 11 (2000) 1.
[16] D.H. Aguilar, L.C. Torres-González, L.M. Torres-Martínez, T. López, P. Quintana, Ciencia UANL VI(1), Enero-Marzo 2003.
[17] A. Morales Acevedo, G.F. Pérez Sánchez, Superficies y Vacío 16 (2003) 18–22.
[18] M.L. Rojas-Cervantes, R.M. Martin-Aranda, A.J. López-Peinado, J. de D. López-Gonzalez, J. Mater. Sci. 29 (1994) 3743–3748.
[19] S. Melada, M. Signoretto, S.A. Ardizzone, C.L. Bianchi, Catal. Lett. 75 (2001) 3–4.
[20] V. Santos, M. Zeni, C.P. Bergmann, J.M. Hohemberger, Rev. Adv. Mater. Sci. 17 (2008) 62–70.
[21] R. Pérez-Hernández, J. Arenas-Alatorre, D. Mendoza-Anaya, A. Gómez-Cortés, G. Díaz, Revista Mexicana de Física 50 (Suplemento 1) (2004) 80–84.
[22] K. Flodström, V. Alfredsson, Micropor. Mesopor. Mater. 59 (2003) 167–176.
[23] R. Huirache-Acuña, B. Pawelec, E. Rivera-Muñoz, R. Nava, J. Espino, J.L.G. Fierro, Appl. Catal. B: Environ. 92 (2009) 168–184.
[24] R. Nava, B. Pawelec, P. Castaño, M.C. Álvarez-Galván, C.V. Loricera, J.L.G. Fierro, Appl. Catal. B: Environ. 92 (2009) 154–167.
[25] D. Brunel, A. Cauvel, F. Fajula, F. Di Renzo, Stud. Surf. Sci. Catal. 97 (1995) 173–180.
[26] P. Mukherjee, M. Sastry, R. Kumar, Phys. Chem. Commun. 3 (2000) 15–17.
[27] T. Martin, A. Galarneau, D. Brunel, V. Izard, V. Hulea, A.C. Blanc, S. Abramson, F. Di Renzo, F. Fajula, Stud. Surf. Sci. Catal. 135 (2001) 4621–4628.
[28] A. Saccà, A. Carbone, R. Pedicini, G. Portable, L. D'Ilario, A. Longo, A. Martorana, E. Passalacqua, J. Membr. Sci. 278 (2006) 105–113.
[29] A. Saccà, A. Carbone, E. Passalacqua, A. D'Epifanio, S. Licoccia, E. Traversa, E. Sala, F. Traini, R. Ornelas, J. Power Sources 152 (2005) 16–21.
[30] A. Carbone, R. Pedicini, A. Saccà, I. Gatto, E. Passalacqua, J. Power Sources 178 (2008) 661–666.
[31] I. Gatto, A. Saccà, A. Carbone, R. Pedicini, F. Urbani, E. Passalacqua, J. Power Sources 171 (2007) 540–545.
[32] M. Guan, W. Liu, Y. Shao, H. Huang, H. Zhang, Micropor. Mesopor. Mater. 123 (2009) 193–201.
[33] D. Zhao, J. Sun, Q. Li, G.D. Stucky, Chem. Mater. 12 (2000) 275–279.
[34] R.G. Rodríguez Avendaño, J.A. De Los Reyes, T. Viveros, J.A. Montoya De La Fuente, Catal. Today 148 (2009) 12–18.
[35] X. Feng, G.E. Fryxell, L.-Q. Wang, A.Y. Kim, J. Liu, K.M. Kemner, Science 276 (1997) 923–926.
[36] J. Liu, X. Feng, G.E. Fryxell, L.-Q. Wang, A.Y. Kim, M. Gong, Chem. Eng. Technol. 21 (1998) 97–100.
[37] C.E. Fowler, S.L. Burkett, S. Mann, Chem. Commun. (1997) 1769–1775.
[38] K. Li, G. Ye, J. Pan, H. Zhang, M. Pan, J. Membr. Sci. 347 (2010) 26–31.
[39] R. Jiang, H. Russell Kunz, J.M. Fenton, J. Membr. Sci. 272 (2006) 116–124.
[40] P. Staiti, A.S. Arico, V. Baglio, F. Lufrano, E. Passalacqua, V. Antonucci, Solid State Ionics 145 (2001) 101–107.
[41] A. Mahreni, A.B. Mohamad, A.A.H. Kadhum, W.R.W. Daud, S.E. Iyuke, J. Membr. Sci. 327 (2009) 32–40.
[42] V. Di Noto, R. Gliubizzi, E. Negro, G. Pace, J. Phys. Chem. B 110 (2006) 24972–24986.
[43] W.J.J. Stevens, V. Meynen, E. Bruijn, O.I. Lebedev, G.V. Tendeloo, P. Cool, E.F. Vansant, Micropor. Mesopor. Mater. 110 (2008) 77–85.